NDT&E International 85 (2017) 72–75

Contents lists available at ScienceDirect

NDT&E International

journal homepage: www.elsevier.com/locate/ndteint

Simulation and inversion of ultrasonic pitch-catch through-tubing well logging with an array of receivers

Erlend Magnus Viggen[a,*], Tonni Franke Johansen[a], Ioan-Alexandru Merciu[b]

[a] SINTEF ICT, Acoustics Research Centre, Trondheim, Norway
[b] Statoil ASA, Research and Technology, Rotvoll, Norway

ARTICLE INFO

Keywords:
Well logging
Ultrasonic pitch-catch measurement
Finite element simulation
Mathematical modelling
Inversion

ABSTRACT

Current methods for ultrasonic pitch-catch well logging use two receivers to log the bonded material outside a single casing. For two casings separated by a fluid, we find by simulation that increasing the number of receivers provides a better picture of the effect of the bonded material outside the second casing. Inverting simulated measurements with five receivers, using a simulated annealing algorithm and a simple forward model, we find for a subset of simulations that we can estimate the impedance of the material outside the outer casing.

1. Introduction

Multiple-casing well logging is a topic of increasing importance, in particular due to the large number of upcoming plug & abandonment operations [1]. Though very little has been published so far on ultrasonic logging in multiple-casing wells [1], ultrasonic logging in single-casing wells has been extensively studied [2–5]. Current methods for single-casing pitch-catch well logging use two receivers, as this is sufficient to measure the exponential attenuation of the primary Lamb wave packet excited on the inner casing. This attenuation can be used to determine the impedance of the bonded material outside the casing [3–5].

In a double-casing geometry as shown in Fig. 1, it has been found [1] that there appears a cascade of leaky Lamb wave packets between the two casings, where later packets feed on earlier ones. The amplitudes of the wave packets and the wavefronts that they emit are proportional. By measuring a wavefront's amplitude, the pitch-catch receivers R_i can thus indirectly measure the relative amplitude of the corresponding wave packet at the time when it emitted the measured part of the wavefront. It has been found [1] that the wave packet amplitudes continuously evolve according to the system geometry and material parameters such as the impedance Z_B of the bonded material in the B-annulus, and that this impedance affects the amplitudes measured by the receivers from later wavefronts.

From these considerations we believe that increasing the number of receivers will improve the possibility and accuracy of inversion to determine the system's parameters, as more points along the packets' evolution are then measured. In this letter we show and discuss results of finite element simulations with five receivers, and demonstrate the possibility of inversion in a subset of the simulated cases.

2. Simulation setup, results, and discussion

Finite element simulations were performed in the system's two-dimensional cross-section. The simulation setup, shown in Fig. 1, is identical to that in [1], with the exception that five receivers are used instead of two. The receivers R_i are positioned 10 cm apart. The first receiver's face centre is 25 cm away from the transmitter's face centre. The number and position of the receivers has not been optimised, but was chosen as a simple extension of [1] with additional receivers that provide information on the later evolution of the wave packets while keeping tool size and computational requirements manageable. The inner casing has a diameter $2a_2 = 7$ in and a thickness $a_2–a_1 = 0.408$ in, while the outer has a diameter $2a_4 = 9\frac{5}{8}$ in and a thickness $a_4–a_3 = 0.545$ in.

As in [1], we restrict ourselves to a simple through-tubing case with water in the interior and the A-annulus, and a variety of materials from Table 1 in the B-annulus. To keep the model simple, and because attenuation is less important for pitch-catch logging except in oil-based muds with very high attenuation, all materials are assumed to be non-attenuating. We discuss the role of attenuation further in Section 3.

The simulation snapshot in Fig. 1 shows the train of leaky Lamb wave packets on both casings, and the leaked wavefronts connecting these. The wavefronts emitted by the packets on the inner casing are measured by the receivers, which filter the impinging pressures and return nondimensionalised signals $S_{R_i}(t)$. Because a wavefront's am-

* Corresponding author.
E-mail address: erlendmagnus.viggen@sintef.no (E.M. Viggen).

http://dx.doi.org/10.1016/j.ndteint.2016.10.008
Received 6 June 2016; Received in revised form 30 August 2016; Accepted 28 October 2016
Available online 04 November 2016

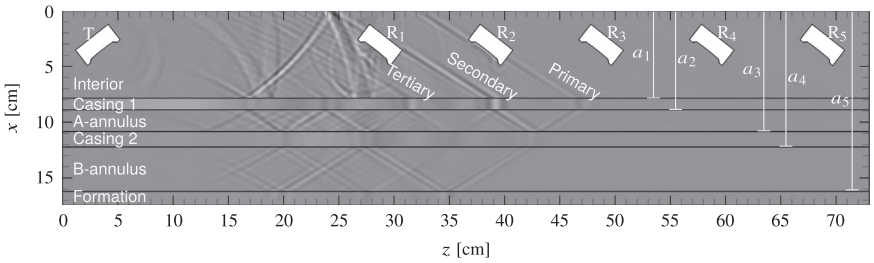

Fig. 1. Snapshot of the simulated system at 170 μs with water in the interior and both annuli, showing pressure in the fluids and x-displacement in the solids.

Table 1
P-wave speed c_p, density ρ, impedance Z, and s-wave speed c_s of simulated materials, taken from [1].

Material	c_p (m/s)	ρ (kg/m^3)	Z (MRayl)	c_s (m/s)
Scree	300	1700	0.51	0
Water	1481	1000	1.48	0
Sat. shales & clays	1200	2050	2.46	0
Foam cement	2250	1330	2.99	767
Sat. shales & sand sect.	1750	2150	3.76	336
Chalk	2400	1900	4.56	897
Marls	2400	2200	5.28	897
Poro. & sat. sandstn.	2600	2300	5.98	1069
Class G cement	3700	1800	6.66	2017
Formation	4645	2200	10.2	2646
Steel casing	5780	7850	45.4	3190

plitude is proportional to its corresponding wave packet's amplitude at the time of emission, the received wavefront signals $S_{R_i}(t)$ shown in Fig. 2a tell of the wave packets' evolution. The peak amplitude corresponding to wavefront k in the envelope of $S_{R_i}(t)$ is denoted as $S_{R_i,k}$.

In Fig. 2a we see that the primary wavefront decreases exponentially that the secondary wavefront peaks between R_1 and R_2, and that the tertiary wavefront decreases and increases in amplitude again from R_3 to R_5. As we will see in Section 3, these phenomenona can be understood through the model presented in [1], and simulated measurements can be used to determine the parameters of this model. With only two receivers as in [1], these phenomena would not have been captured, making it much less feasible determine the physical system from the measurements.

The evolution of the first few wavefronts for various B-annulus materials is shown for the original geometry in Fig. 2b and in c for a modified geometry with equally thick casings (a_4–a_3 = 0.408 in) where the dispersion relations on both casings are very similar. For the original geometry there is a smaller effect of material variation on the secondary and tertiary wavefront, and the same evolution pattern is seen for all materials. For equal casing thicknesses the variation is much stronger on both the secondary and tertiary wavefronts. (To keep Fig. 2c readable, the latter are not shown.) Generally, this matches earlier observations of the outer annulus impedance Z_B having a larger effect on the wave packets for equal casing thicknesses, which may come from the dispersion relations on the casings being more similar so that the wave packets on both casings tend to stay in phase relative to each other [1]. Additionally, we see in both cases that the curves' behaviour is ordered by the B-annulus impedance with the exception of the highest-impedance material. The latter material behaves differently as its p-wave speed c_p is higher than the wave packet speed on the outer casing, which breaks the p-wave coupling [1,3].

We define a logarithmic amplitude ratio, which for steady decay corresponds to attenuation in decibels per unit length, as

$$\alpha_{i,j,k} = \frac{20}{\Delta z_{i,j}} \log\left(\frac{S_{R_i,k}}{S_{R_j,k}}\right) \tag{1}$$

Here, $\Delta z_{i,j} = 10(j-i)$ cm is the distance between transducers R_i and R_j. Only $\alpha_{1,2,1}$ and $\alpha_{1,2,2}$ have previously been examined against Z_B as only two transducers have been available [1]. A plot of amplitude ratios for adjacent receivers R_i and $R_j = R_{i+1}$ is shown for both thickness cases in Fig. 3. We see that the primary wavefronts are in constant steady decay, and in most cases we see that the secondary wavefronts have also

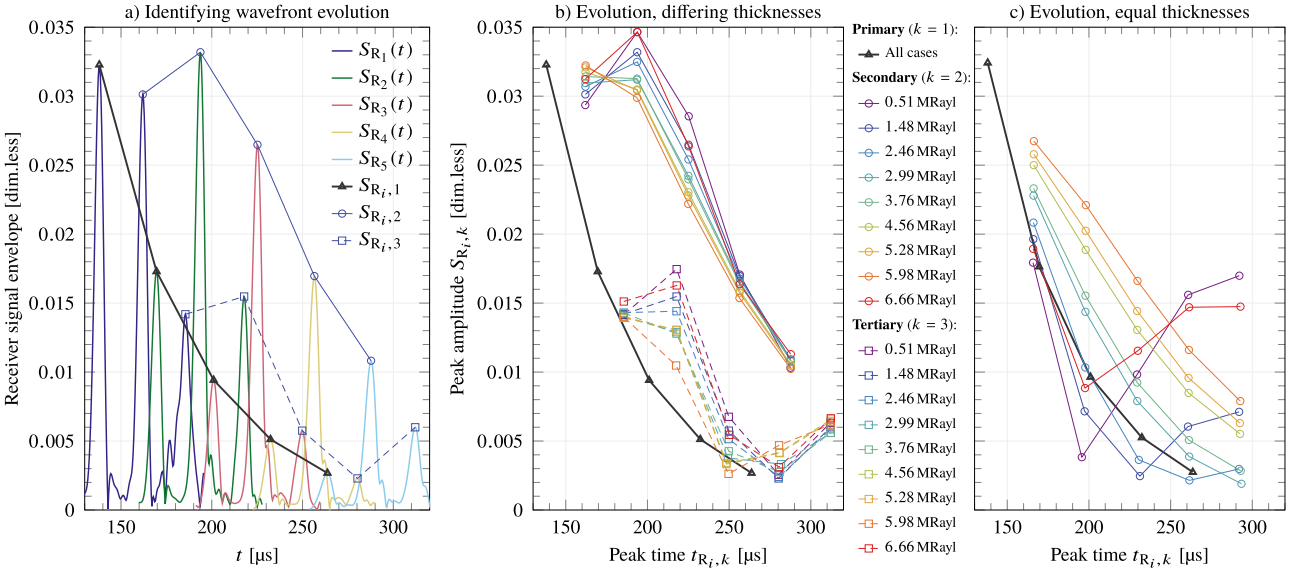

Fig. 2. (a) Envelopes of receiver signals $S_{R_i}(t)$ for water (1.48 MRayl) in the interior and the annuli, along with indicated evolution of primary, secondary, and tertiary wavefronts. (b) Evolution of primary, secondary, and tertiary wavefronts for original casing thicknesses and 9 different B-annulus materials from Table 1, as specified in the legend. (c) Similarly, evolution of primary and secondary wavefronts for equal casing thicknesses.